Reaction frequency of solvated electrons in water interacting with atmospheric-pressure helium plasma jet

Yoshinobu Inagaki[1 *] and Koichi Sasaki[1 †]

[1]*Division of Applied Quantum Science and Engineering, Hokkaido University, Sapporo 060-8628, Japan*

We employed the charge transfer to solvent (CTTS) transition of iodine negative ions to investigate the reactivity of solvated electrons in water interacting with an atmospheric-pressure helium plasma jet. A dye laser pulse at 225 nm was injected into the solution of potassium iodide, which was irradiated with an atmospheric-pressure helium plasma jet, and the reaction frequency of solvated electrons produced by the CTTS transition was measured by optical absorption spectroscopy. We observed the temporal and spatial variations of the reaction frequency of solvated electrons. We found that the reaction frequency of solvated electrons was determined by the concentrations of dissolved oxygen and hydrogen peroxide. We detected a high reaction frequency of solvated electrons in the limited depth region from the solution surface, indicating that hydrogen peroxide is localized near the plasma-liquid interface.

1. Introduction

With the expansion of new plasma applications such as water treatment,[1–3] medicine,[4–6] agriculture,[7–9] and analysis,[10–12] there has been increasing interest in plasma-liquid interaction. In particular, in recent years, there have been increasing challenges for chemical reactions that cannot be seen in either the plasma (gas) phase or the bulk of the liquid phase.[13, 14] It is believed that the unique reactions are originated from the limited region near the plasma-liquid interface. It is speculated that reactive chemical species are concentrated in the limited depth region just below the interface, and they promote the unique reaction processes. The solvated electron is one of such reactive species. The solvated electron is a peculiar electron surrounded by oriented water molecules, and has been studied as one of the simplest quantum solutes since it was first observed in pulse radiolysis in 1962.[15] Many efforts have been paid for understanding the structure and dynamics of solvated electrons in radiation chemistry and biology to unravel the detailed mechanism of genetic damage.[16–18]

In plasma chemistry, solvated electrons were first detected near the interface between

*E-mail: inagaki@eis.hokudai.ac.jp
†Corresponding author, E-mail: sasaki@qe.eng.hokudai.ac.jp

plasma and liquid,[19, 20] and a recent research suggests that they may be involved in various reaction processes of plasma-liquid interaction.[19] However, many hypotheses that are supposed in numerical simulations of plasma-liquid interaction have not been examined by experiments because of the lack of techniques to measure the reactivity of solvated electrons. This is due to the difficulty in the detection of solvated electrons in liquids interacting with plasmas. Rumbach and coworkers succeeded in the detection of hydrated electrons by optical absorption spectroscopy using the total reflection geometry at the plasma-water interface.[19,20] However, this measurement may need delicate optimization of the experimental system, since the vibration of the plasma-water interface may cause serious noise. Probably due to the experimental difficulty, we cannot find further progress in the detection of solvated electrons in liquids interacting with plasmas.

The fundamental reaction processes of solvated electrons are investigated intensively in the field of radiation chemistry using pulse radiolysis. This is a kind of the pump-probe experiment employing a high-energy ($\sim$ 40 MeV) electron accelerator. Solvated electrons are produced instantaneously by pulsed electron impact ionization of the solution, and the temporal decay of the concentration of solvated electrons is measured by optical absorption spectroscopy. However, it is not an easy task to combine an experiment of plasma chemistry with the pulse radiolysis system because of the limited access to the large-scale electron accelerator. In contrast, a similar pump-probe experiment is possible by pulsed laser photolysis, where solvated electrons are produced by photodetachment of solvated halogen and pseudohalogen negative ions.[21] The production process is called the charge transfer to solvent (CTTS) transition. When a pulsed laser with a duration of $\sim$ 10 ns is employed for the light source, the temporal decay of the solvated electron density is measured by the same manner as that in the pulse radiolysis.

In a previous work,[22] we adopted the CTTS transition of iodine negative ions (I^-) to examine the reaction frequency of solvated electrons in an ionic liquid (N,N,N-trimethyl-N-propylammonium bis (trifluoromethylsulfonyl) imide) interacting with a low-pressure argon, oxygen, and nitrogen plasmas. In this work, we carried out a similar experiment in water interacting with an atmospheric-pressure helium plasma jet. We examined the reaction frequency of solvated electrons as a function of the depth from the plasma-liquid interface, and we discussed scavenger chemicals for solvated electrons in water interacting with a helium plasma jet.

2. Experimental method

The experimental setup is schematically shown in Fig. 1. Figure 1(a) was used for the majority of experiments, and we used Fig. 1(b) only for examining the variation of the reaction frequency as a function of the depth from the plasma-liquid interface. The helium plasma jet was generated by dielectric barrier discharge (DBD) in a quartz tube with 4 mm inner diameter. Helium was fed into the quartz tube at a flow rate of 3-9 $\mathrm{Lmin^{-1}}$. Two electrodes were attached on the outside of the quartz tube. An electrode was connected to a high-voltage power supply. The high voltage from the power supply was a bipolar square wave with a voltage of 16-25 kV (peak to peak) and a frequency of 1 kHz. The other electrode was connected to the electrical ground. A quartz cuvette which was filled with potassium iodide (KI) solution was placed at a distance of 10 mm from the end of the quartz tube. The volume of the cuvette was 4.5 mL. We prepared three types of water: ultrapure water (Fujifilm Wako Pure Chemical Corporation), purified water (Asone A300), and tap water (sampled in Hokkaido University). KI was mixed into the water at a concentration of 0.01-0.04 mM. To measure the concentration of dissolved oxygen in the solution, we used a polarographic oxygen meter (Lutron Electronic Enterprise Co., LTD., DO-5519E). When we needed to decrease the concentration of dissolved oxygen in the water, we bubbled nitrogen into the KI solution for 10 min. A concentration of approximately 0.03 mM was possible for dissolved oxygen by the nitrogen bubbling. The differences in Fig. 1(b) from Fig. 1(a) were to employ a funnel which kept a larger amount (60 mL) of KI solution and to provide the flow of sheath oxygen gas around the helium flow. The funnel with a larger amount of KI solution was useful to keep the distance between the solution surface and the end of the quartz tube. The distance was increased with time when the funnel was not employed, since the evaporation of water by the plasma irradiation was not negligible.

To produce solvated electrons, the cuvette with the KI solution was irradiated with a dye laser (Sirah Lasertechnik, CobraStretch) pulse at a wavelength of 225 nm. The duration of the laser pulse was 8 ns. Iodine negative ions (I^-) in the solution were excited to the CTTS band by absorbing laser photons ($I^- + h\nu \rightarrow I^{-*}$), and solvated electrons were produced from I^{-*} ($I^{-*} \rightarrow I + e^-_{solv}$).[21] Optical absorption spectroscopy was adopted for detecting solvated electrons. The light source in absorption spectroscopy was a diode laser (Toptica Photonics, DL100) at a wavelength of 777 nm in all the experiments except the measurement of the absorption spectrum. The dye and diode laser beams were overlapped on the same optical axis using a dichroic mirror. The dye laser beam was terminated using a colored glass plate,

whereas the diode laser beam was detected using a fast Si photodiode (Thorlab, PDA10A2) with a rise time constant of 2.3 ns. The electrical signal from the photodiode was connected to an oscilloscope (Tektronix Inc., DPO2024), and the temporal variation of the transmitted diode laser intensity was recorded after averaging the signal for 16 laser shots to compensate the shot-to-shot reproducibility. We needed to measure the absorption spectrum to confirm that the optical absorption is caused by solvated electrons. The absorption spectrum was measured by using a continuum Xe lamp (Hamamatsu Photonics K.K., L2273) as the light source. The Xe lamp light transmitted through the cuvette was introduced into a monochromator, and the transmitted intensities at various wavelengths were measured using a photomultiplier tube.

3. Results

3.1 Absorbance waveform and spectrum

The typical temporal variations of the absorbance, which is defined by $-\log_{10}(I_t/I_0)$ with I_0 and I_t being the intensities of incident and transmitted Xe lamp light, respectively, are shown in Fig. 2. The origin of the horizontal axis corresponds to the time when the dye laser pulse irradiated the KI solution. We observed the quick increase in the absorbance at the timing of the laser irradiation. The decay of the absorbance observed at 600 nm was approximated well by an exponential function, as shown by the red curve in Fig. 2. On the other hand, we found that the absorbance waveform observed at 780 nm was not approximated by an exponential function. The deviation from the exponential function was apparently seen at a long delay time ($t > 2\ \mu$s). We confirmed that the absorbance spectrum at the tail ($t = 10\ \mu$s) in Fig. 2 agreed with the absorption spectrum of I_2^-.[23] Hence, the optical absorption at the long delay time was attributed partly to I_2^-, which was produced by $I + I^- \rightarrow I_2^-$. Atomic iodine (I) is a product of the CTTS transition. According to a reaction kinetic study,[24] the frequency of $I + I^- \rightarrow I_2^-$ is estimated to be $7 \times 10^5\ s^{-1}$ at the experimental condition. Hence, the concentration of I_2^- was low for a short period after the irradiation of the dye laser pulse, and we approximated the absorbance waveform at $0 \leq t \leq 2\ \mu$s by an exponential function, as shown by the blue curve in Fig. 2. The time constant of the blue exponential function thus determined agreed with that of the red curve. The amplitude of the absorbance waveform is plotted in Fig. 3 as a function of the wavelength. The solid curve shows the absorbance spectrum of solvated electrons in water.[25,26] Since the experimental spectrum agrees with the absorbance spectrum of solvated electrons in water, it is confirmed that the optical absorption is due to solvated electrons produced via the CTTS transition of I^-.

We used the diode laser at 777 nm for measuring the absorbance waveform in all the

experiments except the measurement of the absorption spectrum, since it gave us a higher signal-to-noise ratio than the Xe lamp. The optical absorption at 777 nm is dominated by solvated electrons at the short delay time, as described above. According to the Lambert-Beer law, the absorbance waveform represents the temporal variation of the concentration of solvated electrons. Hence, we deduced the reaction frequency or the reciprocal of the lifetime of solvated electrons by fitting a part ($0 \leq t \leq 2\ \mu$s) of the absorbance waveform with an exponential function. Figure 4 shows the reaction frequency of solvated electrons in the KI solution as a function of the concentration of dissolved oxygen. The plasma jet was not irradiated. As shown in the figure, we observed no significant difference in the reaction frequencies of solvated electrons in the three types of water with different purity. The experimental result suggests that the reaction frequency of solvated electrons in the KI solution is determined by the concentration of dissolved oxygen. The role of dissolved oxygen as a scavenger chemical for solvated electrons will be discussed later.

3.2 Temporal variation of reaction frequency

We observed the temporal variation in the reaction frequency of solvated electrons after the initiation of the plasma irradiation, as shown in Fig. 5. The distance between the solution surface and the measurement position was 10 mm. The flow rate of helium was 3 $\mathrm{Lmin^{-1}}$, and the oxygen sheath gas was not applied in this experiment. It is noted here that the direction of the temporal variation was remarkably dependent on the initial concentration of dissolved oxygen. When the initial concentration of dissolved oxygen was high (when the nitrogen bubbling was not applied), as shown in Fig. 5(a), we observed the temporal decrease in the reaction frequency of solvated electrons by the irradiation of the helium plasma jet at a discharge voltage of 24 kV. We also observed the slight decrease in the reaction frequency of solvated electrons when the solution surface was exposed to the helium flow. In contrast, when the initial concentration of dissolved oxygen was minimized by the nitrogen bubbling, we observed the linear increase in the reaction frequency of solvated electrons, as shown in Fig. 5(b). The slope of the increase was $1.5\times10^5\ \mathrm{s^{-1}min^{-1}}$. This result indicates the production of a scavenger chemical for solvated electrons by the plasma irradiation.

Figure 6 shows the temporal variations of the reaction frequency for a longer time scale. The reaction frequencies observed at two KI concentrations are plotted in the same figure. The initial concentration of dissolved oxygen was minimized by the nitrogen bubbling. The discharge voltage and the flow rate of helium were 24 kV and 3 $\mathrm{Lmin^{-1}}$, respectively. As shown in the figure, the slope of the linear increase in the reaction frequency was independent

of the KI concentration. The increase in the reaction frequency continued for 40 min after the initiation of the plasma irradiation, and after that, we observed a constant reaction frequency of $(6 - 7) \times 10^6\,s^{-1}$. We terminated the plasma irradiation at 60 min, and after that we did not observe the temporal decrease in the reaction frequency, as shown in Fig. 6, even though we continued the helium flow after the termination of the discharge.

3.3 Influence of discharge parameters

Figure 7 shows the difference between the initial reaction frequency and the reaction frequencies at 5 and 10 min after the initiation of the plasma irradiation as a function of the discharge voltage. The initial concentration of dissolved oxygen was minimized by the nitrogen bubbling, and the flow rate of helium was 3 $Lmin^{-1}$. We observed the steep increase in the reaction frequency difference with the discharge voltage, as shown in Fig. 7. Figure 8 shows the difference between the initial reaction frequency and the reaction frequency at 10 min after the initiation of the plasma irradiation as a function of the helium flow rate. The discharge voltage was 24 kV. As shown in the figure, we observed the decrease in the reaction frequency difference with the helium flow rate.

3.4 Spatial variation of reaction frequency

We examined the reaction frequency of solvated electrons as a function of the depth from the solution surface, as shown in Fig. 9. The origin of the horizontal axis is the bottom of the concave meniscus. This experiment was carried out using the apparatus shown in Fig. 1(b). The dye and diode laser beams passed through an iris with a diameter of 0.4 mm to realize a fine spatial resolution. The discharge voltage was 24 kV, and the flow rates of helium and oxygen were 3 $Lmin^{-1}$. The measurements shown in Figs. 9(a) and 9(b) were completed within 10 and 5 min, respectively, after the initiation of the plasma irradiation. It was observed that the reaction frequency in the apparatus shown in Fig. 1(b) was higher than that in Fig. 1(a) in the case without the plasma irradiation, even when we applied the nitrogen bubbling. The experimental result shown in Fig. 9(a) was obtained when the oxygen sheath gas was switched off, *i.e.*, the solution surface was irradiated with the helium flow and the helium plasma jet. The reaction frequency of solvated electrons was low in the region near the solution surface ($\leq$ 1 mm) exposed to the helium flow. We observed the enhancement of the reaction frequency by the plasma irradiation, especially in the region near the solution surface. On the other hand, the depth profile of the reaction frequency was roughly flat when the solution surface was exposed to the flows of helium and oxygen, as shown in Fig. 9(b). When the solution was irradiated with the plasma jet, we found a thin region with a higher reaction frequency of

solvated electrons just below the plasma-liquid interface. The depth of the region with the higher reaction frequency was approximately 0.2 mm. The reaction frequency in the bulk of the KI solution was not affected by the plasma irradiation when we used the apparatus shown in Fig. 1(b).

4. Discussion

4.1 Absolute concentration of solvated electrons

The absolute concentration of solvated electrons produced by the CTTS transition is readily obtained using the Lambert-Beer law with the knowledge of the absorption coefficient. According to the absorption coefficient of $1.9 \times 10^4\ M^{-1}cm^{-1}$ at 720 nm,[27] the concentration of solvated electrons corresponding to the absorbance of 0.1 is 5.2 μM. All the experiments in the present work were carried out at the concentrations of solvated electrons below 5 μM. This concentration is more than one order of magnitude lower than the concentration of dissolved oxygen. In addition, the reaction rate coefficient for a second-order reaction $e^-_{solv} + e^-_{solv} + 2H_2O \rightarrow H_2 + 2OH^-$ is $1.1 \times 10^{10}\ M^{-1}s^{-1}$ (see Table I),[27] corresponding to the reaction frequency on the order of $10^4\ s^{-1}$. These are the reasons for the exponential decrease shown in Fig. 2 or the first-order kinetics of solvated electrons, and in this case the reaction frequency deduced from the exponential curve represents the product of the concentration of the scavenger chemical and the reaction rate coefficient.

4.2 Scavenger chemicals of solvated electrons

The possible scavenger chemicals and their reaction rate coefficients are listed in Table I.[27] The table includes original chemicals in the KI solution and possible reaction products by the plasma-liquid interaction. Short-lived species are excluded from Table I, since we observed the slow increase in the reaction frequency (the slope of the increase was $1.5 \times 10^5\ s^{-1}min^{-1}$) and the constant reaction frequency after the termination of the plasma irradiation. It is understood from Table I that dissolved oxygen can work as the dominant scavenger chemical in the KI solution at a concentration less than 0.04 mM. The solid line illustrated in Fig. 2 represents the reaction frequency predicted by the rate coefficient of $e^-_{solv} + O_2 \rightarrow O_2^-$. The agreement between the experimental results and the value predicted by the rate coefficient indicates the domination of dissolved oxygen in the loss process of solvated electrons in the KI solution. The decrease in the reaction frequency by the exposure to the helium flow (Fig. 5(a)) can be understood by the decrease in the concentration of dissolved oxygen. Similar phenomena have already been discussed in some papers.[28,29]

Ogawa and coworkers reported the production rates of stable chemicals in water irradiated

with a helium plasma jet, as shown in Table II.[30] The volume of the cuvette they used in their experiment was the same as that in our experiment. They observed the decrease in the concentration of dissolved oxygen by the plasma irradiation. The loss rate was dependent on the initial concentration of dissolved oxygen. Our experimental result shown in Fig. 5(a), which shows the decrease in the reaction frequency of solvated electrons with time when the nitrogen bubbling is not applied, is consistent with the decrease in the concentration of dissolved oxygen by the plasma irradiation. On the other hand, we should suppose the production of other scavenger chemicals to explain the increase in the reaction frequency of solvated electrons when the initial concentration of dissolved oxygen is minimized (Figs. 5(b) and 6). Ogawa and coworkers reported the production rates of H_2O_2, NO_2^-, and NO_3^- as shown in Table II. Table II also shows the products of the production rates P and the rate coefficients k of their reactions with solvated electrons. These values predict the increase rates in the reaction frequency of solvated electrons. Therefore, on the basis of the observation by Ogawa and coworkers, it is considered that H_2O_2 is the most important scavenger chemical for solvated electrons in water irradiated with the helium plasma jet. The increase rate in the reaction frequency we observed (1.5×10^5 $s^{-1}min^{-1}$) corresponds to 1.4×10^{-5} $Mmin^{-1}$ for the production rate of H_2O_2, which agrees with the value shown in Table II within a factor of 2.3. The steep increase in the reaction frequency difference with the discharge voltage (Fig. 7) is explained by the increase in the concentration of H_2O_2. The decrease in the reaction frequency difference with the helium flow rate (Fig. 8) is also reasonable, since the sources of H_2O_2 are considered to be molecular oxygen and water vapor admixed into the helium plasma jet from ambient air. We observed the increase in the reaction frequency even when we applied the oxygen sheath gas (Fig. 9(b)), suggesting that nitrogen oxides are less important than H_2O_2 as scavenger chemicals for solvated electrons.

The depth profiles of the reaction frequency of solvated electrons, which are shown in Fig. 9, are also understood by the reactions with dissolved oxygen and H_2O_2. The higher reaction frequency in the apparatus shown in Fig. 1(b) than Fig. 1(a) is due to a higher concentration of dissolved oxygen in the KI solution which is kept in the large-volume funnel. The depth profile in the absence of the plasma jet is determined by the profile of the concentration of dissolved oxygen. The concentration of dissolved oxygen near the solution surface is low when the solution surface is exposed to the helium flow (Fig. 9(a)), whereas it becomes flat when the solution surface is exposed to the flows of helium and oxygen (Fig. 9(b)). The irradiation of the plasma jet enhanced the reaction frequency near the solution surface, indicating that H_2O_2 has a high concentration in the limited depth region from the

solution surface. This is reasonable since the production processes of H_2O_2 are the transport from the plasma and the reaction $OH + OH \rightarrow H_2O_2$ at the plasma-liquid interface. The volume-averaged H_2O_2 concentration is lower in the apparatus shown in Fig. 1(b) because of the larger volume of the solution. This is the reason why the reaction frequency in the bulk of the solution is not affected by the plasma irradiation.

4.3 Influence of KI

We should discuss the influence of KI on the reaction kinetics of solvated electrons, since KI is admixed into water as the source of solvated electrons but it is not present in the normal plasma-liquid interaction. The direct influence is the reactions with I^- and other iodine compounds. For example, the production of I_3^- is observed in a KI-starch solution irradiated with an atmospheric-pressure plasma jet,[31] and the reaction rate coefficient of I_3^- is relatively large in the chemicals listed in Table I. However, we observed the same reaction frequency of solvated electrons at different KI concentrations, as shown in Fig. 6. Since the KI concentration in the present experiment was 0.01-0.04 mM, considering the rate coefficients listed in Table I, iodine compounds cannot be major scavenger chemicals for solvated electrons. Another possibility of the influence of KI on the reaction kinetics is the reaction between H_2O_2 and I^- ($H_2O_2 + 2H^+ + 3I^- \rightarrow 2H_2O + I_3^-$). However, this possibility is basically denied by Fig. 6, where we observed the same reaction frequency at different KI concentrations. In addition, we estimated the effective reaction rate coefficient for the $H_2O_2 + I^-$ reaction at the experimental conditions (the solution temperature between 15 and 25 °C and the pH value between 6 and 8) by referring to literature.[32] The estimated rate coefficient was $\sim$ 0.5 $M^{-1}s^{-1}$, corresponding to a reaction rate of $\sim 3 \times 10^{-7}$ $Mmin^{-1}$ for H_2O_2 and I^- concentrations being 0.5 and 0.02 mM, respectively. The H_2O_2 concentration of 0.5 mM is the value at 30 min after the initiation of the plasma irradiation. Since the reaction rate of $\sim 3 \times 10^{-7}$ $Mmin^{-1}$ is much lower than the production rate of H_2O_2, the H_2O_2 concentration is not affected by the reaction with I^-.

5. Conclusions

In this work, we employed the CTTS transition of I^- to investigate the reaction frequency of solvated electrons in water interacting with an atmospheric-pressure helium plasma jet. The reaction frequency of solvated electrons was determined by the concentrations of dissolved oxygen and H_2O_2. The plasma irradiation had opposite effects on dissolved oxygen and H_2O_2. We observed the decrease in the reaction frequency of solvated electrons or the decrease in the concentration of dissolved oxygen, when the initial concentration of dissolved oxygen was

high. In contrast, when the initial concentration of dissolved oxygen was low, we observed the increase in the reaction frequency due to the production of H_2O_2 by the plasma-liquid interaction. We detected a high reaction frequency of solvated electrons in the limited depth region from the solution surface, indicating that H_2O_2 is localized near the plasma-liquid interface.

Acknowledgment

The authors would like to thank Naoki Shirai for useful discussion. This work was supported by JSPS KAKENHI (19K21861 and 20H00135).

References

1) T. Miichi, N. Hayashi, S. Ihara, S. Satoh and C. Yamabe, Ozone Sci. Eng. **24**, 471 (2002).
2) Z. Stará and F. Krčma, Czech. J. Phys. **54**, C1050 (2004).
3) B. R. Locke, M. Sato, P. Sunka, M. R. Hoffmann and J.-S. Chang, Ind. Eng. Chem. Res. **45**, 882 (2006).
4) G. Fridman, G. Friedman, A. Gutsol, A. B. Shekhter, V. N. Vasilets and A. Fridman, Plasma Processes and Polymers **5**, 503 (2008).
5) M. G. Kong, G. Kroesen, G. Morfill, T. Nosenko, T. Shimizu, J. van Dijk and J. L. Zimmermann, New J. Phys. **11**, 115012 (2009).
6) K.-D. Weltmann, M. Polak, K. Masur, T. von Woedtke, J. Winter and S. Reuter, Contributions to Plasma Physics **52**, 644 (2012).
7) B. Šerá, I. Gajdová, M. Šerý and P. Špatenka, Plasma Sci. Technol. **15**, 935 (2013).
8) R. Thirumdas, A. Kothakota, U. Annapure, K. Siliveru, R. Blundell, R. Gatt and V. P. Valdramidis, Trends Food Sci. Technol. **77**, 21 (2018).
9) S. Perni, D. W. Liu, G. Shama and M. G. Kong, J. Food Prot. **71**, 302 (2008).
10) N. Shirai, S. Uchida and F. Tochikubo, Plasma Sources Sci. Technol. **23**, 054010 (2014).
11) P. Rumbach, A. E. Lindsay and D. B. Go, Plasma Sources Sci. Technol. **28**, 105014 (2019).
12) Y. E. Kovach, M. C. García and J. E. Foster, IEEE Trans. Plasma Sci. **47**, 3214 (2019).
13) N. Shirai, G. Suga and K. Sasaki, J. Phys. D: Appl. Phys. **52**, 39LT02 (2019).
14) S. Kanazawa, H. Kawano, S. Watanabe, T. Furuki, S. Akamine, R. Ichiki, T. Ohkubo, M. Kocik and J. Mizeraczyk, Plasma Sources Sci. Technol. **20**, 034010 (2011).
15) E. J. Hart and J. W. Boag, J. Am. Chem. Soc. **84**, 4090 (1962).
16) A. T. Shreve, T. A. Yen and D. M. Neumark, Chem. Phys. Lett. **493**, 216 (2010).
17) J. M. Herbert and L. D. Jacobson, J. Phys. Chem. A **115**, 14470 (2011).
18) M. P. Coons, Z.-Q. You and J. M. Herbert, J. Am. Chem. Soc. **138**, 10879 (2016).
19) P. Rumbach, D. M. Bartels, R. M. Sankaran and D. B. Go, Nat. Commun. **6**, 7248 (2015).
20) P. Rumbach, D. M. Bartels, R. M. Sankaran and D. B. Go, J. Phys. D: Appl. Phys. **48**, 424001 (2015).
21) M. J. Blandamer and M. F. Fox, Chem. Rev. **70**, 59 (1970).
22) Y. Inagaki and K. Sasaki, Jpn. J. Appl. Phys. **59**, 066001 (2020).

23) A. J. Elliot and F. C. Sopchyshyn, Int. J. Chem. Kinet. **16**, 1247 (1984).
24) A. Treinin and E. Hayon, Int. J. Radiat. Phys. Chem. **7**, 387 (1975).
25) F.-Yuan. Jou and G. R. Freeman, J. Phys. Chem. **83**, 2383 (1979).
26) D. M. Bartels, K. Takahashi, J. A. Cline, T. W. Marin and C. D. Jonah, J. Phys. Chem. A **109**, 1299 (2005).
27) G. V. Buxton, C. L. Greenstock, W. P. Helman and A. B. Ross, J. Phys. Chem. Ref. Data **17**, 513 (1988).
28) J.-S. Oh, E. J. Szili, N. Gaur, S.-H. Hong, H. Furuta, H. Kurita, A. Mizuno, A. Hatta and R. D. Short, J. Phys. D: Appl. Phys. **49**, 304005 (2016).
29) J.-S. Oh, X. Strudwick, R. D. Short, K. Ogawa, A. Hatta, H. Furuta, N. Gaur, S.-H. Hong, A. J. Cowin, H. Fukuhara, K. Inoue, M. Ito, C. Charles, R. W. Boswell, J. W. Bradley, D. B. Graves and E. J. Szili, Appl. Phys. Lett. **109**, 203701 (2016).
30) K. Ogawa, J.-S. Oh, N. Gaur, S.-H. Hong, H. Kurita, A. Mizuno, A. Hatta, R. D. Short, M. Ito and E. J. Szili, Jpn. J. Appl. Phys. **58**, SAAB01 (2019).
31) A. Nakajima, G. Uchida, T. Kawasaki, K. Koga, T. Sarinont, T. Amano, K. Takenaka, M. Shiratani and Y. Setsuhara, J. Appl. Phys. **118**, 043301 (2015).
32) H. A. Liebhafsky and A. Mohammad, J. Am. Chem. Soc. **55**, 3977 (1933).

Table I. Rate coefficients k for reactions between solvated electrons and various chemicals.[27)]

Chemical	Rate coefficient k ($M^{-1}s^{-1}$)
H^+	2.3×10^{10}
H_2O	1.9×10^{1}
H_2O_2	1.1×10^{10}
HOI	2.0×10^{10}
I^-	$< 2.4 \times 10^{5}$
I_2	5.3×10^{10}
I_3^-	3.5×10^{10}
IO^-	1.6×10^{10}
IO_3^-	7.8×10^{9}
K^+	$< 5 \times 10^{5}$
NO_2^-	4.1×10^{9}
NO_3^-	9.7×10^{9}
O_2	1.9×10^{10}

Table II. Production rates P of H_2O_2, NO_2^-, NO_3^-, and O_2 reported by Ogawa and coworkers.[30] The products of the production rates P and their rate coefficients k for their reactions with solvated electron are also listed.

Chemical	Production rate P ($Mmin^{-1}$)[30]	kP ($s^{-1}min^{-1}$)
H_2O_2	5.8×10^{-6}	6.4×10^{4}
NO_2^-	9.4×10^{-7}	3.8×10^{3}
NO_3^-	7.0×10^{-7}	6.8×10^{3}
O_2	$-3.1 \times 10^{-5} \leq P \leq 0$*	$-5.9 \times 10^{5} \leq kP \leq 0$*

*Depends on concentration

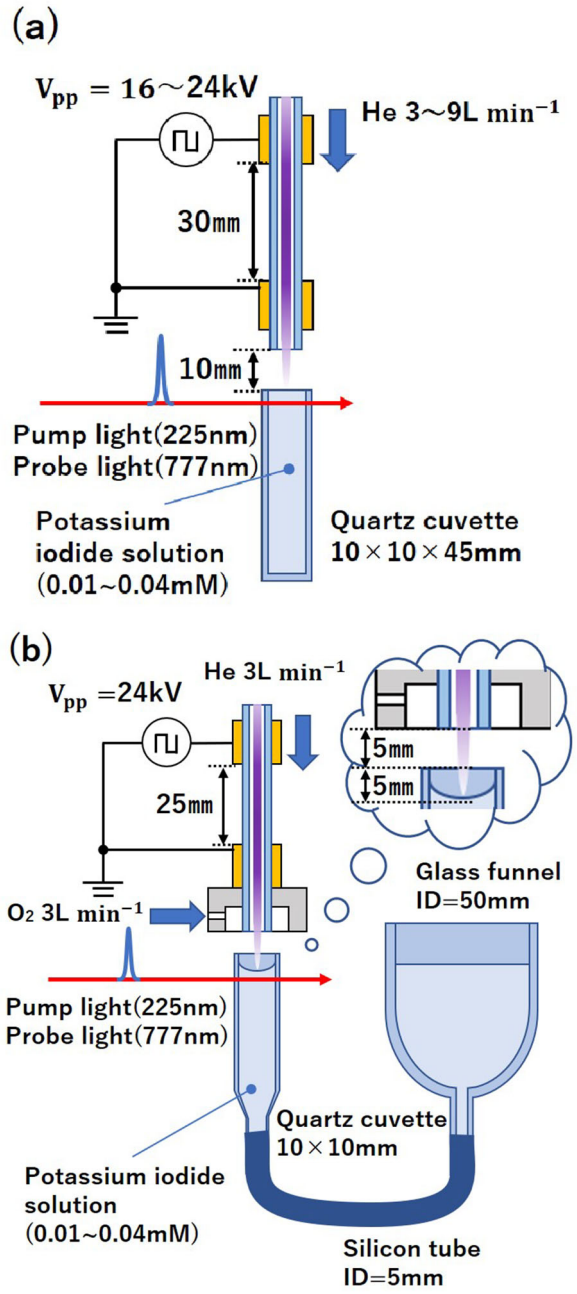

Fig. 1. Experimental setup.

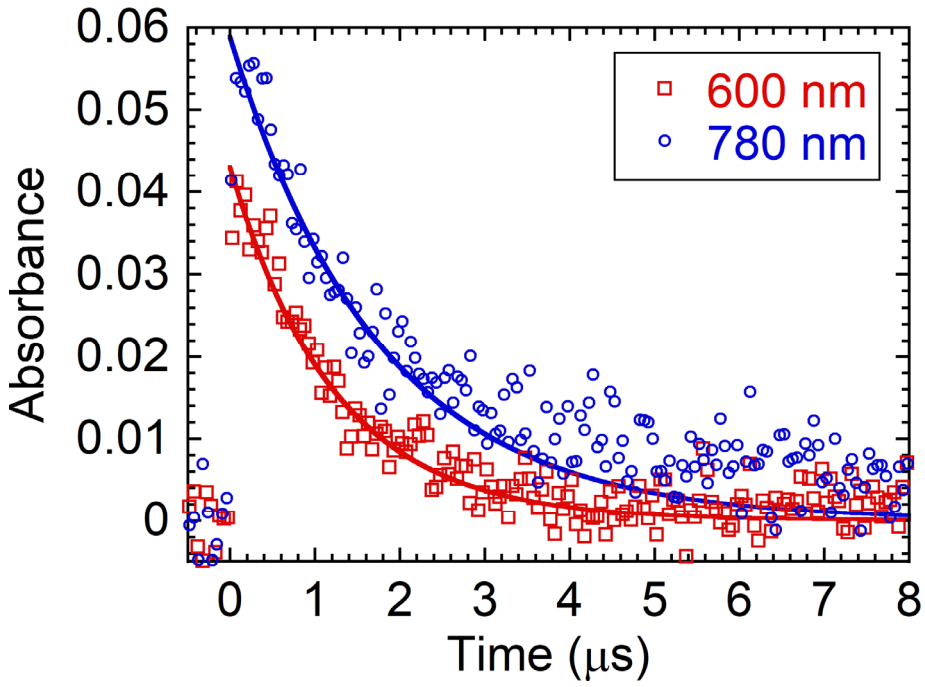

Fig. 2. Temporal variations of absorbances at 600 and 780 nm. The dye laser pulse is injected at $t = 0$ μs. The solid curves show the fitting between the experimental data at $0 \leq t \leq 2$ μs and exponential functions.

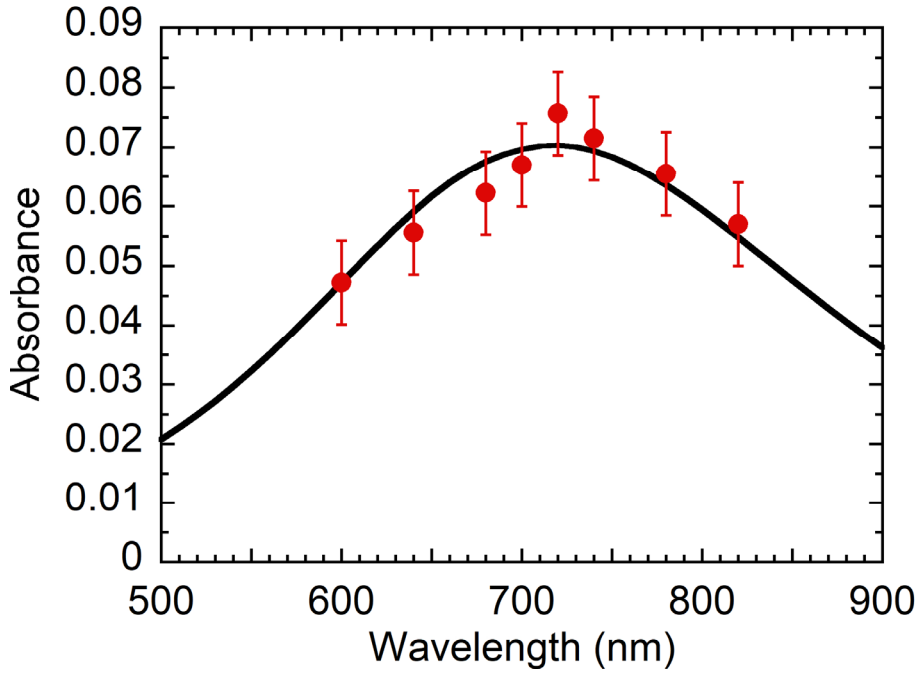

Fig. 3. Relationship between the peak absorbance and the wavelength. The solid curve is the absorbance spectrum of solvated electrons in water at 298 K.[25,26)]

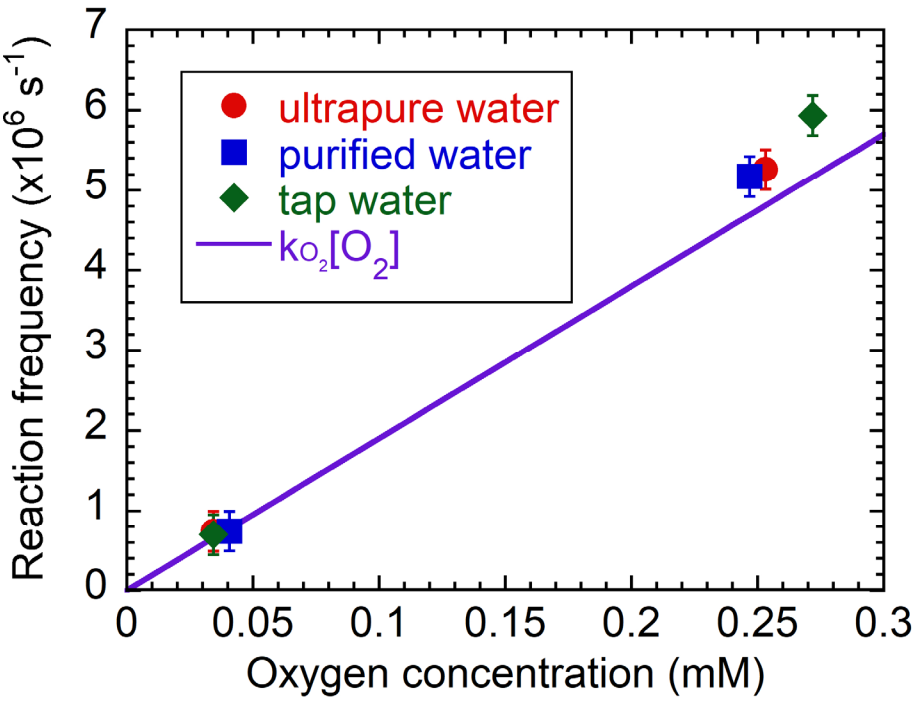

Fig. 4. Reaction frequency of solvated electrons as a function of the concentration of dissolved oxygen. The solid line represents the reaction frequency predicted by the rate coefficient of $e^-_{solv} + O_2 \rightarrow O_2^-$.

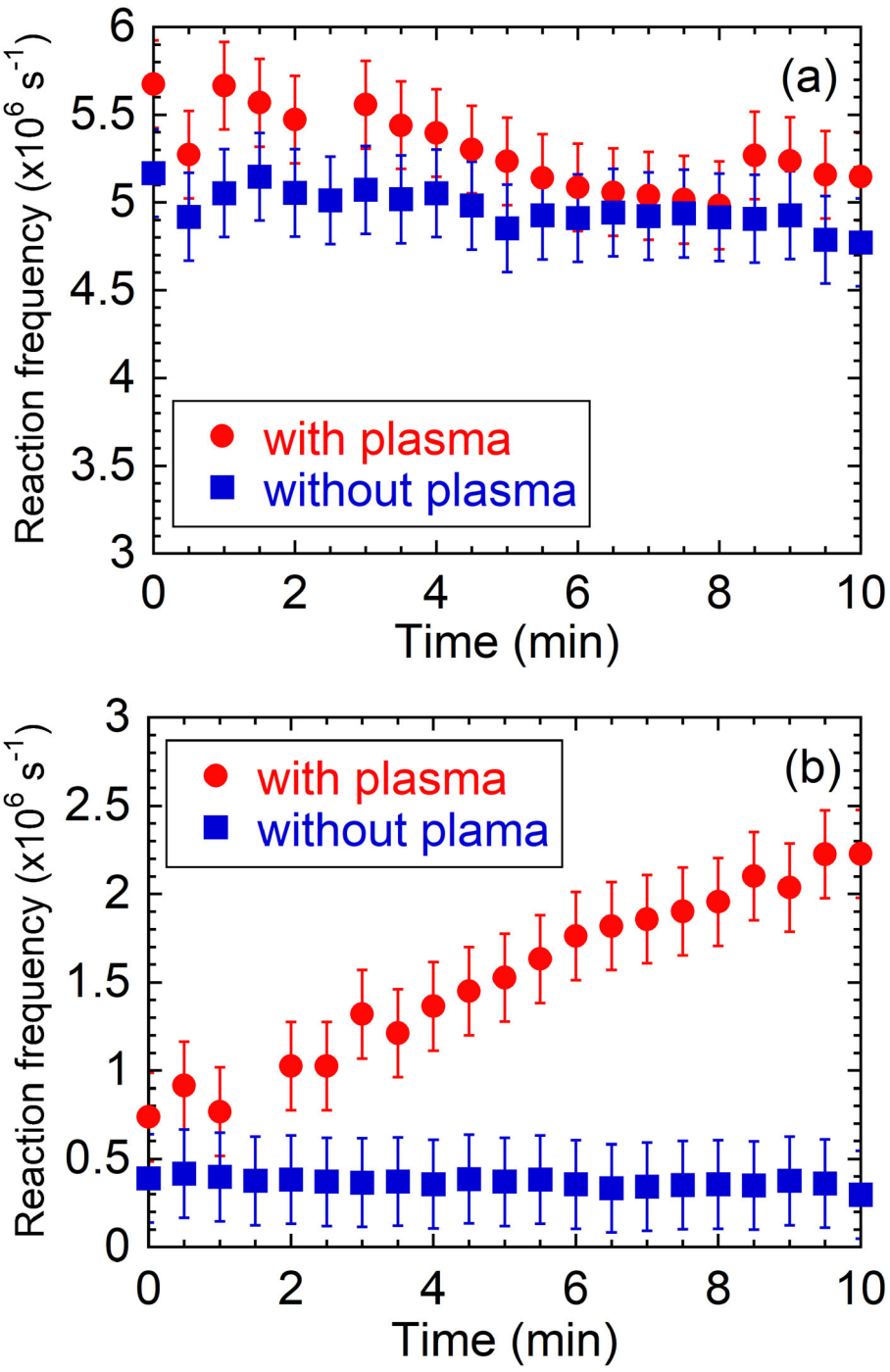

Fig. 5. Temporal variations of the reaction frequency of solvated electrons after the initiation of the plasma irradiation. The nitrogen bubbling was not applied in (a), whereas the concentration of dissolved oxygen was minimized by the nitrogen bubbling in (b).

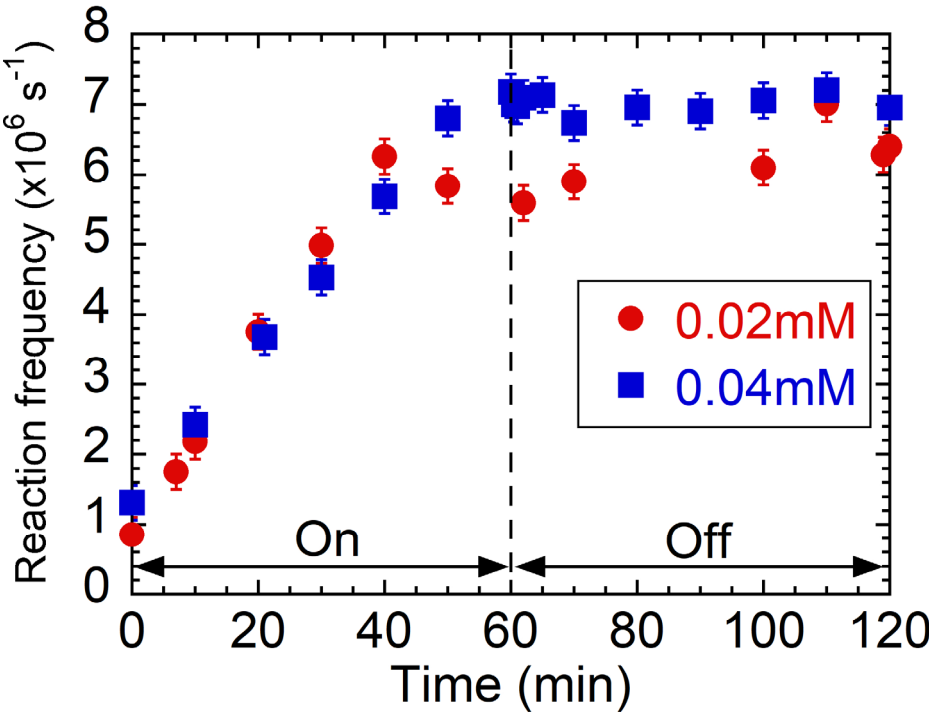

Fig. 6. Temporal variations of the reaction frequency of solvated electrons during the plasma irradiation and after the termination of the plasma irradiation. The duration of the plasma irradiation was 60 min. Reaction frequencies observed at two KI concentrations are plotted.

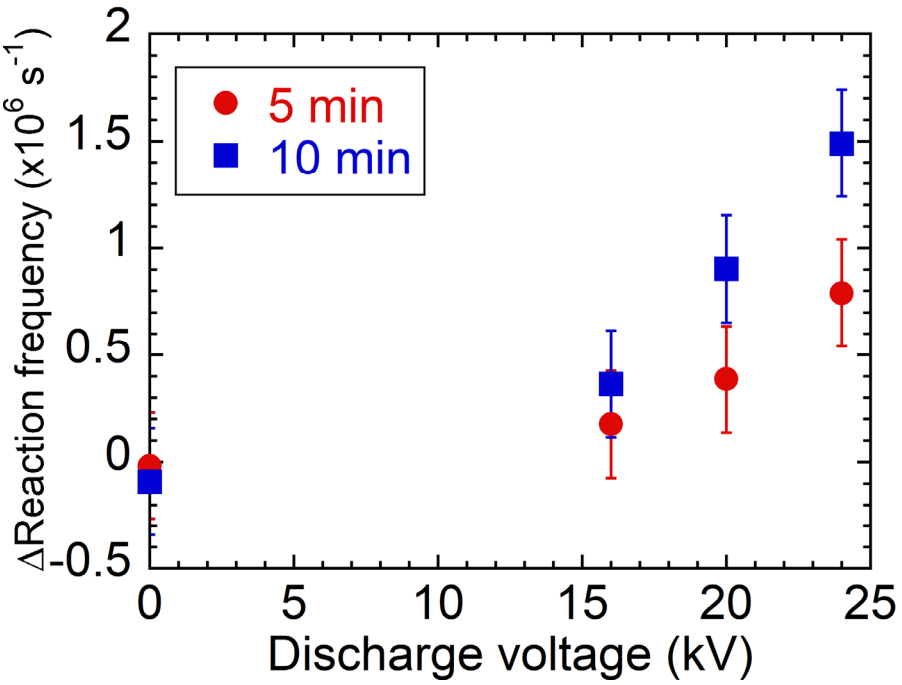

Fig. 7. Difference between the initial reaction frequency and the reaction frequencies at 5 and 10 min after the initiation of the plasma irradiation as a function of the discharge voltage.

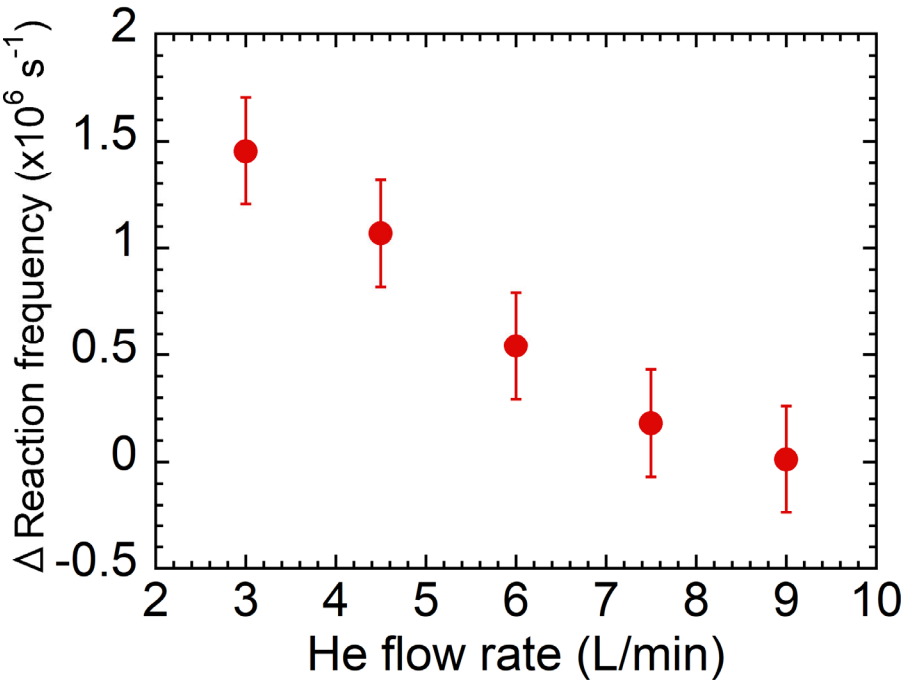

Fig. 8. Difference between the initial reaction frequency and the reaction frequency at 10 min after the initiation of the plasma irradiation as a function of the flow rate of helium.

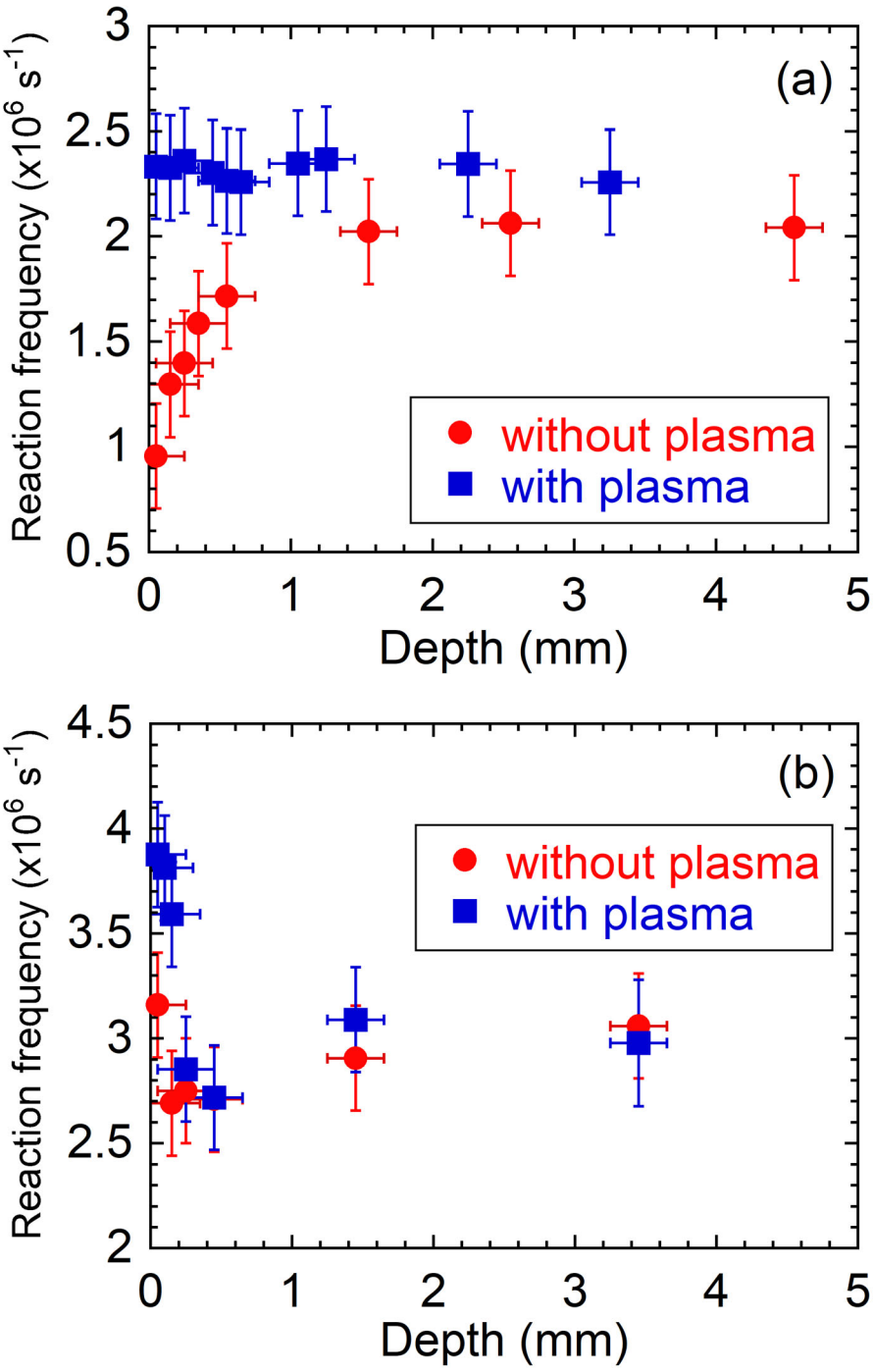

Fig. 9. Depth profiles of the reaction frequency of solvated electrons. (a) was obtained in the presence and absence of the plasma irradiation when the oxygen sheath gas around the helium flow was not applied. (b) was obtained by the similar experiment to (a) but the oxygen sheath gas around the helium flow was applied. Measurements shown in (a) and (b) were completed within 10 and 5 min, respectively, after the initiation of the plasma irradiation.